Acta Oceanol. Sin., 2021, Vol. 40, No. 4, P. 127–135
https://doi.org/10.1007/s13131-021-1845-8
http://www.hyxb.org.cn
E-mail: ocean2@hyxb.org.cn

A second order random wave model for predicting the power performances of a wave energy converter

Yingguang Wang[1, 2,*]

[1] State Key Laboratory of Ocean Engineering, Shanghai Jiao Tong University, Shanghai 200240, China

[2] School of Naval Architecture, Ocean and Civil Engineering, Shanghai Jiao Tong University, Shanghai 200240, China

Received 22 December 2019; accepted 16 May 2020

Abstract

The power performances of a point absorber wave energy converter (WEC) operating in a nonlinear multi-directional random sea are rigorously investigated. The absorbed power of the WEC Power-Take-Off system has been predicted by incorporating a second order random wave model into a nonlinear dynamic filter. This is a new approach, and, as the second order random wave model can be utilized to accurately simulate the nonlinear waves in an irregular sea, avoids the inaccuracies resulting from using a first order linear wave model in the simulation process. The predicted results have been systematically analyzed and compared, and the advantages of using this new approach have been convincingly substantiated.

Key words: absorbed power, wave energy converters, Power-Take-Off, second order wave model, realistic sea

Citation: Wang Yingguang. 2021. A second order random wave model for predicting the power performances of a wave energy converter. Acta Oceanologica Sinica, 40(4): 127–135, doi: 10.1007/s13131-021-1845-8

1 Introduction

Ocean wave energy refers to the harnessing of the herculean power of ocean waves. Ocean waves hold a gargantuan amount of untapped energy, some of which we can use to power at least a portion of the world's everyday electricity. The ocean wave energy has the advantages of being highly predictable, renewable and eco-friendly. An engineering device utilized for exploiting the ocean wave power is called a wave energy converter (WEC). In order to successfully design a wave energy converter, accurately simulating the random ocean waves in the WEC dynamic analysis process is of uttermost importance. However, until present, the majority of the people in the worldwide wave energy research community have applied simple linear irregular waves in their WEC dynamic simulation processes (Manuel et al., 2018; Sirnivas et al., 2016; Tom et al., 2016, 2018, 2019). The linear irregular wave model has the disadvantages that it can only generate unrealistic waves with horizontal symmetries, i.e., the generated waves have statistically symmetric wave crests and troughs. This linear wave model is only suitable for approximately simulating random waves from a very mild sea state in a very deep sea. However, real world ocean waves will become statistically asymmetric (i.e., having sharper and higher crests but smoother and shallower troughs) in a harsh deep sea or at a shallow water coastal site.

Fernandes and Fonseca (2013) has pointed out that most of the proposed WECs will be installed and operated in shallow water coastal sites where the water depths are less than 90 m. Because the ocean waves in these shallow water sites will become statistically asymmetric, the linearly simulated statistically symmetric waves obviously should not be used as the inputs in the analysis and design of most of the proposed WECs.

In order to generate shallow water random waves with statistical asymmetries, Lindgren (2015) and Wang (2019) applied quasi-linear wave models for simulating the movements of individual water particles. However, the random wave simulations presented in Lindgren (2015) and Wang (2019) assumed that wave energy is traveling in only one direction (considered the same direction as the wind). That is to say, Lindgren (2015) and Wang (2019) had respectively performed their stochastic wave simulations based on a uni-directional wave spectrum. Similarly, when Wang (2018a, b) and Wang and Wang (2018) used nonlinear wave models for studying the power performances of wave energy converters, they also applied uni-directional wave spectra during their stochastic simulation of asymmetric waves.

In the real world, however, wind-generated ocean wave energy does not necessarily propagate in the same direction as the wind; instead, the ocean wave energy usually spreads over various directions. Therefore, for an accurate description of random seas, it is necessary to clarify the spreading status of energy. The wave spectrum representing energy in a specified direction is called the directional spectrum, denoted by $S(\omega, \theta)$. Obviously, the energy of a sea state characterized by the wave spectrum $S(\omega, \theta)$ continuously varies as the wave frequency ω and direction θ changes. However, to the best of this author's knowledge, in the current literature, there exists no research work that has performed nonlinear wave simulations based on a multi-directional spectrum during the power performance analysis of wave energy converters.

Motivated by the aforementioned facts, in this paper the power performances of a WEC operating in a nonlinear random sea characterized by a multi-directional spectrum $S(\omega, \theta)$ will be rigorously investigated. The absorbed power of the WEC Power-

Foundation item: The National Natural Science Foundation of China under contract No. 51979165.
*Corresponding author, E-mail: wyg110@sjtu.edu.cn

Take-Off system will be predicted by incorporating a second order random wave model into a nonlinear dynamic filter. This will be a new approach, and, as the second order random wave model can be utilized to accurately simulate the nonlinear waves in an irregular multi-directional sea, avoids the inaccuracies resulting from using a first order linear wave model in the simulation process. The predicted results in this paper will be systematically analyzed and compared, and the advantages of using this new approach will finally be substantiated.

The reminder of this paper will be organized as follows: In Section 2 the theories behind the second order random wave simulation based on a multi-directional spectrum will be elucidated, and the measured wave elevation data from a multi-directional coastal sea will be utilized to validate the accuracies of the second order nonlinear random wave simulation method. In Section 3 the theoretical background of the nonlinear dynamic filter of a wave energy converter will be provided. In Section 4 the calculation results of some specific calculation examples will be presented and discussed, with concluding remarks finally summarized in Section 5.

2 The theories and validation of a second order random wave simulation method

2.1 *The theories of the second order random wave simulation method*

The fluid region is described by using the 3D Cartesian coordinates (x, y, z), with x the longitudinal coordinate, y the transverse coordinate, and z the vertical coordinate (positive upwards). Time is denoted by t. The location of the free surface is at $z=\eta(x, y, t)$ at a specific time of t.

For real fluid flows in the sea surface, it is reasonable to neglect the effects of viscosity. Meanwhile, sea water has a low compressibility, and therefore normally sea water flows are incompressible. Considering the aforementioned facts, it is reasonably accurate to assume that the fluids on the sea surface are ideal (i.e., incompressible and inviscid). Furthermore, rotation of a fluid particle can be caused only by a torque applied by shear forces on the sides of the particle. Since shear forces are absent in an ideal fluid, the flow of ideal fluids is essentially irrotational. Then, the velocity potential $\Phi(x, y, z, t)$ exists. If the water depth d at the sea bottom is constant, then for constant water depth d, the velocity potential $\Phi(x, y, z, t)$ and the free surface elevation $\eta(x, y, t)$ can be determined by solving the following boundary value problem:

$$\nabla^2\Phi = 0, \tag{1}$$

$$\frac{\partial\Phi}{\partial t} + \frac{1}{2}(\nabla\Phi)^2 + gz = 0, \quad z = \eta(x, y, t). \tag{2}$$

$$\frac{\partial\eta}{\partial t} + \frac{\partial\Phi}{\partial x}\frac{\partial\eta}{\partial x} + \frac{\partial\Phi}{\partial y}\frac{\partial\eta}{\partial y} - \frac{\partial\Phi}{\partial z} = 0, \quad z = \eta(x, y, t). \tag{3}$$

$$\frac{\partial\Phi}{\partial z} = 0, \quad z = -d. \tag{4}$$

In this study the following expansion is utilized to solve the system (1)–(4):

$$\begin{cases} \Phi = \Phi^{(1)} + \Phi^{(2)} + \ldots \\ \eta = \eta^{(1)} + \eta^{(2)} + \ldots \end{cases}, \quad \frac{\Phi^{(n+1)}}{\Phi^{(n)}} = \frac{\eta^{(n+1)}}{\eta^{(n)}} O(\varepsilon), \tag{5}$$

where ε is a small parameter which is typically proportional to the wave steepness. For an irregular sea state characterized by a specific wave spectrum $S_{\eta\eta}(\omega)$ in which ω denotes the angular frequency, it can be shown that a first order linear solution of the system (1)–(4) can be expressed as follows:

$$\Phi^{(1)}(x, t) = \mathrm{Re}\sum_{n=1}^{N} \frac{\mathrm{i}gc_n}{\omega_n} \frac{\cosh k_n(z+d)}{\cosh k_n d} \mathrm{e}^{i(\omega_n t - k_n x + \varepsilon_n)}, \tag{6}$$

$$\eta^{(1)}(x, t) = \mathrm{Re}\sum_{n=1}^{N} c_n \mathrm{e}^{i(\omega_n t - k_n x + \varepsilon_n)}, \tag{7}$$

where N is usually chosen to be a sufficiently large positive integer, i stands for the imaginary unit, c_n denotes the sinusoidal wave component amplitude, ε_n is the phase angle uniformly distributed in the interval $[0, 2\pi]$, ω_n denotes the radian frequency ($\omega_n = 2\pi n/T$, T is the time interval) and k_n denotes the wave number. ω_n and k_n are related through the following linear dispersion relation:

$$\omega_n{}^2 = gk_n \tanh(k_n d), \tag{8}$$

where d and g are respectively the water depth and the gravitational acceleration.

Equation (7) describes an ideal linear irregular sea model and this model has been derived under the assumption that the wave heights are small compared to the wave length. Then, the surface elevation resulting from irregular ocean waves can be approximated as a superposition of multiple harmonic waves with different amplitudes and phases. Furthermore, in this ideal linear irregular sea model the random phase angles, ε_n are assumed to be uniformly distributed between 0 and 2π. However, for modelling shallow water nonlinear waves, the above linear irregular sea model should be corrected by including second order terms as follows:

$$\Phi^{(2)}(x, t) = 2\mathrm{Re}\sum_{n=1}^{N}\sum_{m=-1}^{N} \mathrm{i}c_n c_m P(\omega_n, \omega_m) \frac{\cosh(k_n + k_m)(z+d)}{\cosh(k_n + k_m)d} \times \mathrm{e}^{i(\omega_n t - k_n x + \varepsilon_n)} \mathrm{e}^{i(\omega_m t - k_m x + \varepsilon_n)} + 2\sum_{n=1}^{N} \frac{c_n{}^2 g k_n}{\sinh 2k_n h} t, \tag{9}$$

$$\eta^{(2)}(x, t) = \mathrm{Re}\sum_{m=1}^{N}\sum_{n=1}^{N} c_m c_n \times \left(r_{mn} \mathrm{e}^{i(\omega_m t - k_m x + \varepsilon_m + \omega_n t - k_n x + \varepsilon_n)} + q_{mn} \mathrm{e}^{i(\omega_m t - k_m x + \varepsilon_m - \omega_n t + k_n x - \varepsilon_n)} \right). \tag{10}$$

The terms $P(\omega_n, \omega_m)$, r_{mn} and q_{mn} in Eqs (9) and (10) are called quadratic transfer functions, and there expressions are given as follows:

$$P(\omega_n,\omega_m)=(1-\delta_{-n,m})\frac{\frac{g^2k_nk_m}{2\omega_n\omega_m}-\frac{1}{4}\left({\omega_n}^2+{\omega_m}^2+\omega_n\omega_m\right)+\frac{g^2}{4}\frac{\left(\omega_n{k_m}^2+\omega_m{k_n}^2\right)}{\omega_n\omega_m\left(\omega_n+\omega_m\right)}}{\left(\omega_n+\omega_m\right)-g\frac{k_n+k_m}{\left(\omega_n+\omega_m\right)}\tanh\left(\left(k_n+k_m\right)d\right)}, \tag{11}$$

$$r_{mn}=-\left(\frac{1}{g}\right)\left(\frac{\left(\frac{1}{4\omega_m\omega_n}\right)2\left(\omega_m+\omega_n\right)\left({\omega_n}^2{\omega_m}^2-k_mk_mg^2\right)+\omega_n\left({\omega_m}^4-g^2{k_m}^2\right)+\omega_m\left({\omega_n}^4-g^2{k_n}^2\right)}{\left(\omega_m+\omega_n\right)^2\cosh\left(\left(k_m+k_n\right)d\right)-g\left(k_m+k_n\right)\sinh\left(\left(k_m+k_n\right)d\right)}\right)\times$$
$$\left(\omega_m+\omega_n\right)\cosh\left(\left(k_m+k_n\right)d\right)-\left(\frac{1}{4g\omega_m\omega_n}\right)\left(k_mk_ng^2-{\omega_n}^2{\omega_m}^2\right)+\left(\frac{1}{4g}\right)\left({\omega_m}^2+{\omega_n}^2\right), \tag{12}$$

$$q_{mn}=-\left(\frac{1}{g}\right)\left(\frac{\left(\frac{1}{4\omega_m\omega_n}\right)2\left(\omega_m-\omega_n\right)\left({\omega_n}^2{\omega_m}^2+k_mk_mg^2\right)-\omega_n\left({\omega_m}^4-g^2{k_m}^2\right)+\omega_m\left({\omega_n}^4-g^2{k_n}^2\right)}{\left(\omega_n-\omega_m\right)^2\cosh\left(\left|k_m-k_n\right|d\right)-g\left|k_n-k_m\right|\sinh\left(\left|k_n-k_m\right|d\right)}\right)\times$$
$$\left(\omega_n-\omega_m\right)\cosh\left(\left|k_n-k_m\right|d\right)-\left(\frac{1}{4g\omega_m\omega_n}\right)\left(k_mk_ng^2+{\omega_n}^2{\omega_m}^2\right)+\left(\frac{1}{4g}\right)\left({\omega_m}^2+{\omega_n}^2\right), \tag{13}$$

where the Kroenecker delta ($\delta_{-n,m}$=1, if n+m = 0, 0 otherwise) is introduced to avoid a singular $P(\omega_n,\omega_m)$. The wave surface elevations for the second order nonlinear waves can finally be obtained by combining Eq. (7) and Eq. (10) as follows:

$$\eta(x,t)=\eta^{(1)}(x,t)+\eta^{(2)}(x,t)=\mathrm{Re}\sum_{n=1}^{N}c_n\mathrm{e}^{i(\omega_nt-k_nx+\varepsilon_n)}+$$
$$\mathrm{Re}\sum_{m=1}^{N}\sum_{n=1}^{N}c_mc_n\left(r_{mn}\mathrm{e}^{i(\omega_mt-k_mx+\varepsilon_m+\omega_nt-k_nx+\varepsilon_n)}+\right.$$
$$\left.q_{mn}\mathrm{e}^{i(\omega_mt-k_mx+\varepsilon_m-\omega_nt+k_nx-\varepsilon_n)}\right). \tag{14}$$

The proposed second order random wave simulation method starts with taking a multi-directional spectrum $S(\omega,\theta)$ and integrating the energy over all directions to give the total energy at each frequency. The obtained equivalent frequency spectrum $S(\omega)$ is then utilized to generate a nonlinear wave elevation time series by applying Eqs (8) and (14) at a specific site of the sea. Finally it should be pointed out that the coefficients c_n (or c_m) in Eq. (14) are determined by using a given spectrum $S(\omega)$ as follows:

$$c_n=\sqrt{2S(\omega)\Delta\omega}, \tag{15}$$

where $\Delta\omega=\omega_C/N$, and ω_C is the upper cut off frequency beyond which the wave spectrum $S(\omega)$ may be assumed to be 0 for either mathematical or physical reasons.

As we know, a wave spectrum is actually obtained from the observed time series of water elevation. The transformation from water elevation to wave spectrum is based on the assumption that irregular waves can be treated as a combination of linear waves with different amplitudes, different frequencies and different phases. It would be better to give an explanation for how to reasonably consider the nonlinearity of waves in the inverse transformation (i.e., the transformation from the wave spectrum to the nonlinear water elevation). In the following, we will raise a specific calculation example of this inverse transformation.

This study shows as an example to use Eq. (7) to simulate the linear Gaussian wave time histories of a sea state with a JONSWAP spectrum with a significant wave height H_S= 6 m, a spectral peak period T_p=8 s, a peakedness factor γ=1 and corresponding to a water depth of 10 m.

Figure 1 shows our simulation of the linear part wave elevation time series $\eta^{(1)}(x,t)$ which contains 150 wave elevation points (with an equal time distant of 0.1 s between two successive points). A wave elevation point has two coordinates (the first coordinate is time, and the second coordinate is the value of the wave elevation above the mean water level). The computation is based on Eq. (7) and the aforementioned JONSWAP spectrum.

Figure 2 shows our simulation of the second order correction part wave elevation time series $\eta^{(2)}(x,t)$ which contains 150 wave elevation points (with an equal time distant of 0.1 s between two successive points). The computation is based on Eq. (10) and the aforementioned JONSWAP spectrum. This is precisely an example for how to reasonably consider the nonlinear correction part of waves in the inverse transformation (i.e., the transformation from the wave spectrum to the nonlinear correction part water elevation).

In Fig. 3 the blue curve shows our simulation of the entire $\eta(x,t)$ (the linear part $\eta^{(1)}(x,t)$ plus the second order correction part $\eta^{(2)}(x,t)$) wave elevation time series which contains 150 wave elevation points (with an equal time distant of 0.1 s between two successive points). The computation is based on Eq. (14) and the aforementioned JONSWAP spectrum. In Fig. 3, the red curve shows our simulation of the linear part wave elevation time series $\eta^{(1)}(x,t)$ which contains 150 wave elevation points based on the aforementioned JONSWAP spectrum. In Fig. 3, the green curve shows our simulation of the second order correction part wave elevation time series $\eta^{(2)}(x,t)$ which contains 150 wave elevation

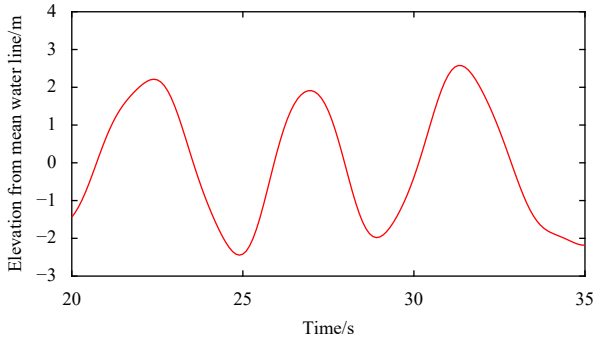

Fig. 1. The simulation of the linear part $\eta^{(1)}(x,t)$ which contains 150 wave elevation points.

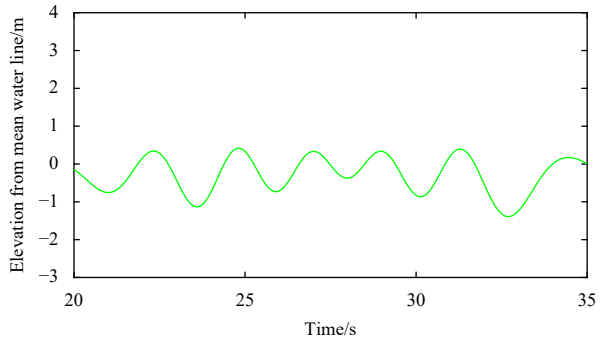

Fig. 2. The simulation of the second order correction part $\eta^{(2)}(x,t)$ which contains 150 wave elevation points.

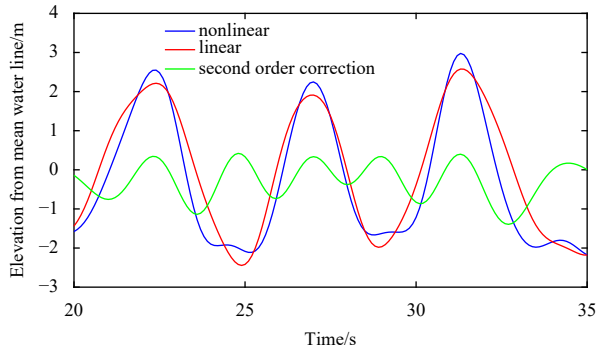

Fig. 3. The simulations of the blue curve entire nonlinear waves $\eta(x,t)$, the red curve linear waves $\eta^{(1)}(x,t)$ and the green curve second order correction waves $\eta^{(2)}(x,t)$, respectively, of 150 points of wave elevation time series.

points based on the aforementioned JONSWAP spectrum. We can see that the wave crests of the entire nonlinear waves $\eta(x,t)$ have become steeper and higher. This is a precise example for how to reasonably consider the nonlinearity of the entire waves in the inverse transformation (i.e., the transformation from the wave spectrum to the entire nonlinear waves).

2.2 *The validation of the proposed second order random wave simulation method*

In this sub-section, the accuracy of the proposed second order random wave simulation method will be validated by a calculation example. Specifically, the proposed second order random wave simulation method will be applied for calculating the wave crest amplitude exceedance probabilities of a sea state with a multi-directional wave spectrum based on the measured surface elevation data at the coast of Yura. The measured surface elevation data at the coast of Yura were obtained at a location 3 km off Yura fishing harbor facing the Sea of Japan. The observations were carried out during the period from 11:10 am to 2:08 pm on November 24, 1987 by the Ship Research Institute, Ministry of Transport of Japan. Temporal sea surface elevations were measured with ultrasonic-type wave gages installed at three points in 42 m water depth. The sampling time interval during the measurement was 1 s. Based on these measured Yura coast surface elevation data, a multi-directional wave spectrum was estimated by using the Maximum Likelihood Method and is shown in Fig. 4. Fig. 5 shows a part of the measured wave elevation time series by the mid-point wave gage at this site.

In the field of ocean engineering, based on a specific wave spectrum, an empirical (or theoretical) model or numerical simulation methods can be used to calculate the exceedance probabilities of the wave crest amplitudes (which is directly related to the occurrence probability of the extreme waves). In the following, taking the multi-directional wave spectrum in Fig. 4 as a calculation example, this study will test the proposed second order random wave simulation method to calculate the exceedance probabilities of the wave crest amplitudes, and compare its accuracy with those of a theoretical model or a linear simulation method.

Figure 6 shows the calculated wave crest amplitudes exceedance probabilities based on the multi-directional spectrum shown in Fig. 4 and the measured Yura coast wave data. The continuous green curve in Fig. 6 represents the calculation results of the wave crest amplitudes exceedance probabilities directly obtained from the measured Yura coast wave data that contains 10 700 wave elevation points. This continuous green curves based on the measured Yura coast wave data are used as the benchmark against the accuracy of the results from the various numerical simulation methods and from an existing theoretical wave crest amplitudes model which is checked.

The continuous red curve in Fig. 6 represents the results of the wave crest amplitudes exceedance probabilities obtained from using the theoretical Rayleigh distribution model expressed as follows:

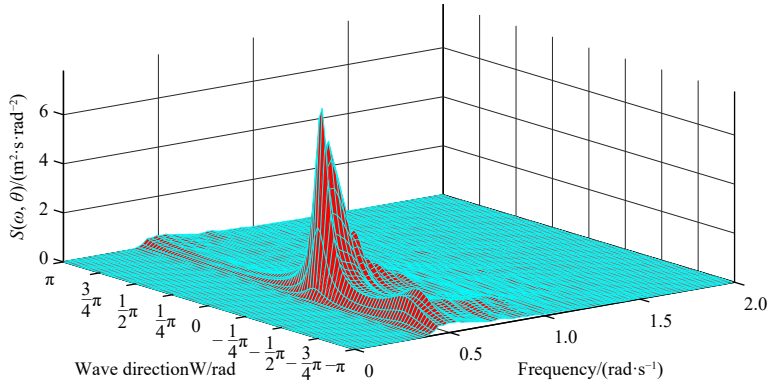

Fig. 4. A multi-directional wave spectrum from the measured data at the coast of Yura.

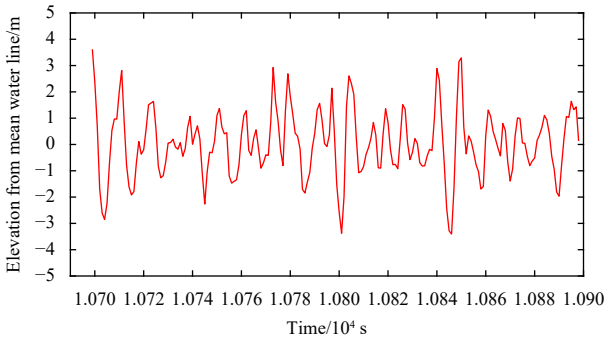

Fig. 5. A part of the measured wave elevation time series at the coast of Yura.

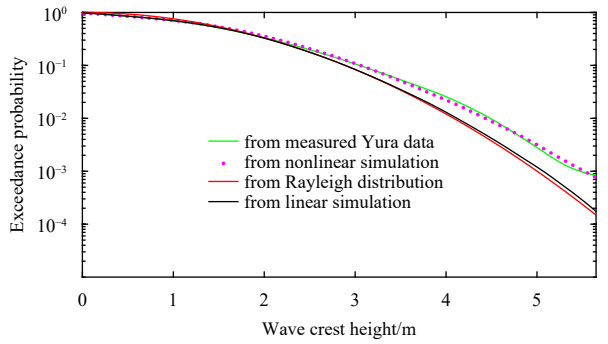

Fig. 6. Comparison between the wave crest amplitudes exceedance probabilities from the linear simulation, from the Rayleigh distribution, from the nonlinear simulation, and the wave crest amplitudes exceedance probabilities results from the measured Yura coast wave data.

$$P\left(A_{\mathrm{c}}>h\right)=\exp\left(-8\left(\frac{h}{H_{\mathrm{S}}}\right)^{2}\right), \tag{16}$$

where h represents the wave crest amplitude, H_{S} represents the significant wave height, A_{c} represents crest amplitude. The wave crest amplitudes exceedance probabilities obtained from using the theoretical Rayleigh distribution model deviate a lot from the corresponding benchmark results obtained directly from the measured Yura coast wave data. This is not a surprise because the theoretical Rayleigh distribution is an ideal linear model and the measured Yura coast wave elevation series are obviously nonlinear. The continuous black curve in Fig. 6 represents the results of the wave crest amplitude exceedance probabilities obtained from using the linear simulation method based on the multi-directional spectrum shown in Fig. 4. The linear simulation process started with taking the multi-directional spectrum shown in Fig. 4 and integrating the energy over all directions to give the total energy at each frequency. The obtained equivalent frequency spectrum was then used to generate a wave elevation time series of 800 000 points by applying Eqs (7) and (8). Next, the wave crest amplitudes time series were extracted from these 800 000 wave elevation points. Finally, the wave crests amplitudes exceedance probabilities were obtained by statistical and mathematical processing the extracted wave crest amplitudes time series. Obviously, the wave crest amplitudes exceedance probabilities obtained from using the linear simulation method also deviate substantially from the corresponding benchmark results obtained directly from the measured Yura coast wave data.

In order to more accurately calculate the wave crest amplitudes exceedance probabilities, the proposed second order random wave simulation method was tried to use. In Fig. 6, a pink * represents the result of the wave crest amplitudes exceedance probability obtained from using the proposed second order random wave simulation method based on the multi-directional spectrum shown in Fig. 4. The proposed second order random wave simulation process started with taking the multi-directional spectrum shown in Fig. 4 and integrating the energy over all directions to give the total energy at each frequency. The obtained equivalent frequency spectrum was then utilized to generate a nonlinear wave elevation time series of 800 000 points by applying Eqs (8) and (14). Next, the wave crest amplitudes time series were extracted from these 800 000 wave elevation points. Finally, the wave crests amplitudes exceedance probabilities were obtained by statistical and mathematical processing the extracted wave crest amplitudes time series. Note that in the figure legend the phrase “from nonlinear simulation” exactly means “from second order random wave simulation”. The wave crest amplitudes exceedance probabilities obtained from using the proposed second order random wave simulation method fit quite well with the corresponding benchmark results obtained directly from the measured Yura coast wave data. The accuracy of the proposed second order random wave simulation method is therefore convincingly validated.

3 The theoretical background of the nonlinear dynamic filter of a wave energy converter

In the practice ocean engineering, the power performances prediction of a WEC is usually carried out by inputting simulated ocean waves in a nonlinear dynamic filter and performing subsequent time domain simulations. The mathematical equations of the WEC nonlinear dynamic filter are written as follows:

$$\begin{aligned}\boldsymbol{M}_{\mathrm{RB}}\ddot{\boldsymbol{x}}\left(t\right)=&-\boldsymbol{A}\left(\infty\right)\ddot{\boldsymbol{x}}\left(t\right)-\int_{0}^{t}\bar{\boldsymbol{K}}\left(t-\tau\right)\dot{\boldsymbol{x}}\left(\tau\right)\mathrm{d}\tau+\\&\boldsymbol{P}_{\mathrm{wave}}\left(t\right)+\boldsymbol{P}_{\mathrm{ext}}\left(t\right)+\boldsymbol{P}_{\mathrm{visc}}\left(t\right)-\boldsymbol{P}_{\mathrm{hs}},\end{aligned} \tag{17}$$

where $\boldsymbol{M}_{\mathrm{RB}}$ is the WEC rigid body inertia matrix and $\boldsymbol{x}\left(t\right)$ is the WEC position. Meanwhile, $\boldsymbol{A}\left(\infty\right)$ is the WEC infinite-frequency added mass matrix and $\bar{\boldsymbol{K}}\left(t\right)$ is the kernel function. $\boldsymbol{P}_{\mathrm{wave}}\left(t\right)$, $\boldsymbol{P}_{\mathrm{ext}}\left(t\right)$, $\boldsymbol{P}_{\mathrm{visc}}\left(t\right)$ and $-\boldsymbol{P}_{\mathrm{hs}}$ are the wave excitation, external, hydrodynamic viscous and hydrostatic loads (forces and moments) respectively.

In the field of ocean engineering, the WEC hydrodynamic memory effects are captured in Eq. (17) by the convolution integral term that is a function of $\dot{\boldsymbol{x}}\left(\tau\right)$ and the kernel functions $\bar{\boldsymbol{K}}\left(t\right)$ which are related to the WEC radiation damping. Meanwhile in Eq. (17), the external load $\boldsymbol{P}_{\mathrm{ext}}\left(t\right)$ represent the Power-Take-Off system forces and moments.

However, up until present, the wave excitation load $\boldsymbol{P}_{\mathrm{wave}}\left(t\right)$ in the WEC dynamic filter are typically calculated by using linearly simulated irregular waves as inputs. As pointed out in Section 1, the linear irregular wave model has the disadvantages that it can only generate unrealistic waves with horizontal symmetries. Even though some researchers (Lindgren, 2015; Wang, 2018a, b, 2019; Wang and Wang, 2018) had tried to use quasi-linear wave models or nonlinear wave models for simulating irregular waves with statistical asymmetries, all these researchers unfortunately performed their stochastic wave simulations based

on some unrealistic uni-directional wave spectra. Therefore, Section 1 illustrated the extension of these research work is needed very much in order to study the power performances of a wave energy converter in a multi-directional random sea. Motivated by these facts, in the present study, the wave excitation load $\boldsymbol{P}_{\text{wave}}(t)$ was calculated by inputting nonlinearly simulated irregular waves based on a multi-directional wave spectrum. In the next section, some calculation examples regarding the power performances of a point absorber wave energy converter operating in a multi-directional random sea will be presented.

4 Some specific calculation examples and calculation result discussion

4.1 *The point absorber wave energy converter*

Our specific calculation examples will be carried out regarding a heaving two-body point absorber wave energy converter. Figure 7 shows this specific wave energy converter modeled in WEC-Sim (http://wec-sim.github.io/WEC-Sim/), an open source computer software for simulating WEC performances. The dimensions of this specific wave energy converter are shown in Fig. 8. This two-body point absorber WEC consists of a float and a spar/plate. The float has a diameter of 20 m, a thickness of 5 m and a mass of 727.01 t. The spar has a height of 38 m and a diameter of 6 m. The spar/plate has a mass of 878.3 t.

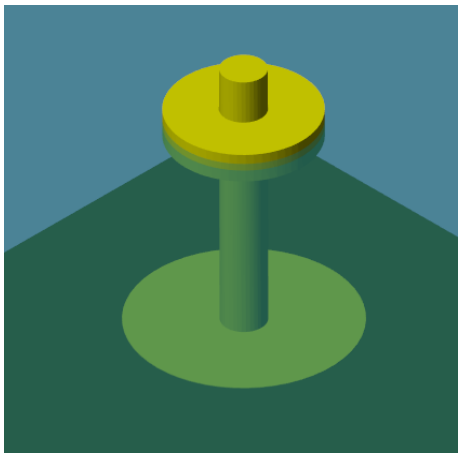

Fig. 7. The WEC-Sim model of the chosen heaving two-body point absorber.

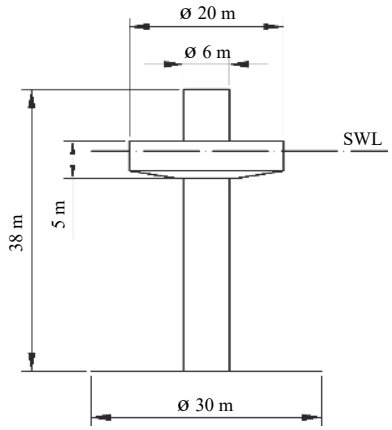

Fig. 8. The main dimensions of the chosen heaving two-body point absorber. SWL represents still water line.

It should be emphasized that this two-body point absorber WEC is installed in a coastal sea area with a water depth of only 49.5 m. Obviously, the random waves in this shallow water area will be nonlinear according to the nonlinear random wave theory in Ochi (1998).

4.2 *Some specific calculation examples and calculation result discussion*

In most wave energy exploitation engineering projects that met in the real world, the only information knew beforehand regarding a sea state usually will be a specific wave spectrum. In Section 2, the accuracy of the proposed second order random wave simulation method was already demonstrated in generating irregular waves based on a measured multi-directional wave spectrum. In the following calculation examples, the proposed second order random wave simulation method was utilized for generating nonlinear irregular waves for calculating the wave excitation load $\boldsymbol{P}_{\text{ext}}(t)$ in Eq. (17). The absorbed power of the aforementioned WEC Power-Take-Off system was predicted for some specific sea states characterized with multi-directional JONSWAP spectra. Figure 9 shows one of these multi-directional JONSWAP spectra with a significant wave height H_S=1 m, a spectral peak period T_p=12 s, a peakedness factor γ=1, and a cosine squared spreading function with the spreading parameter equal to 15. The mathematical expression of this multi-directional JONSWAP spectrum is as follows:

$$S(\omega,\theta)=S(\omega)D(\theta), \tag{18}$$

where $S(\omega)$ is a frequency spectrum and $D(\theta)$ is a spreading function.

The mathematical expression for the frequency spectrum $S(\omega)$ is as follows (Wang, 2014):

$$S(\omega)=5.061\frac{g^2}{\omega^5}\frac{{H_S}^2}{{T_p}^4}(1-0.287\ln(\gamma))\times \exp\left(-\frac{5}{4}\left(\frac{\omega T_p}{2\pi}\right)^{-4}\right)\gamma^{\exp\left(-0.5\left(\frac{\left(\frac{\omega T_p}{2\pi}-1\right)^2}{\delta^2}\right)\right)}, \tag{19}$$

where $\delta=0.07$, if $\omega<2\pi/T_p$; $\delta=0.09$, if $\omega\geqslant 2\pi/T_p$. ω is the wave angular frequency.

$$\gamma=\exp(3.484(1-0.197\,5(0.036-0.005\,6T_p/\sqrt{H_S})T_p{}^4/H_S{}^2)). \tag{20}$$

The mathematical expression for the spreading function $D(\theta)$ in Eq. (18) is as follows:

$$D(\theta)=\frac{\Gamma(s+1)}{2\sqrt{\pi}\Gamma(s+1/2)}\cos^{2s}\left(\frac{\theta}{2}\right), \tag{21}$$

where the spreading parameter s=15.

Figure 10 is a corresponding polar plot of the multi-directional JONSWAP spectrum as shown in Fig. 9.

Next, the calculation results of the absorbed power of the aforementioned wave energy converter were placed in an ideal linear sea versus in a multi-directional nonlinear random sea. Figure 11 shows the predicted WEC absorbed power time series under the sea state of linear irregular waves based on a multi-dir-

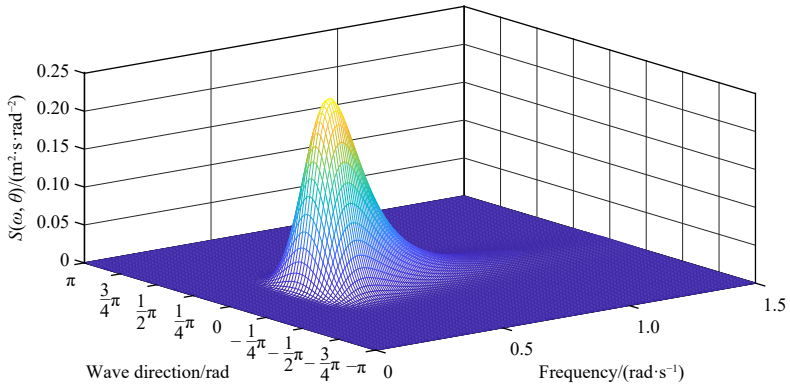

Fig. 9. A multi-directional JONSWAP wave spectrum with H_S=1 m, T_p=12 s, γ=1, and a cosine squared spreading function with the spreading parameter equal to 15.

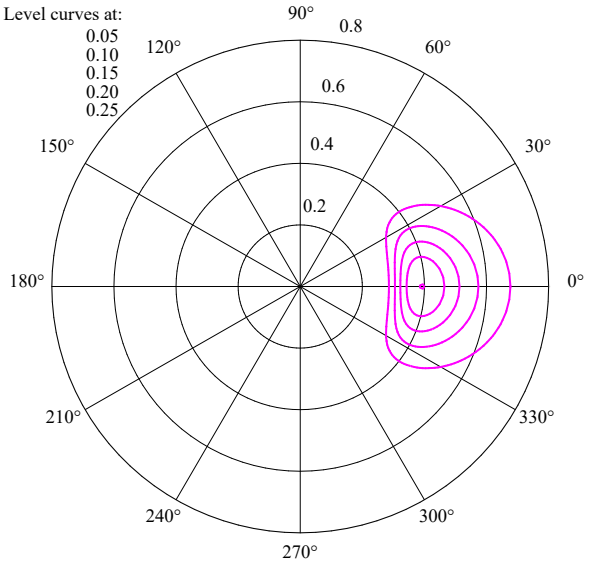

Fig. 10. A corresponding polar plot of the multi-directional JONSWAP spectrum as shown in Fig. 9.

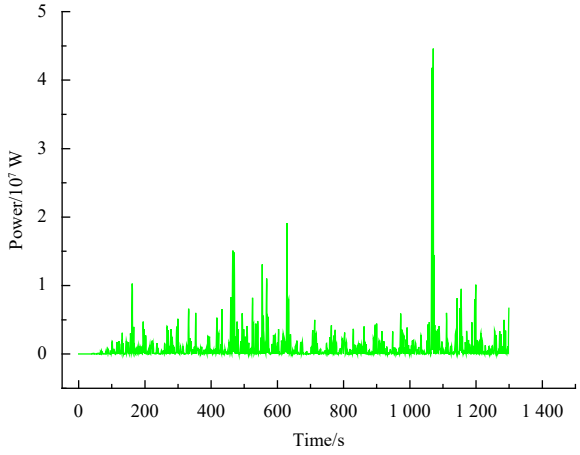

Fig. 11. WEC absorbed power time series under the sea state of linear waves with H_S=12 m.

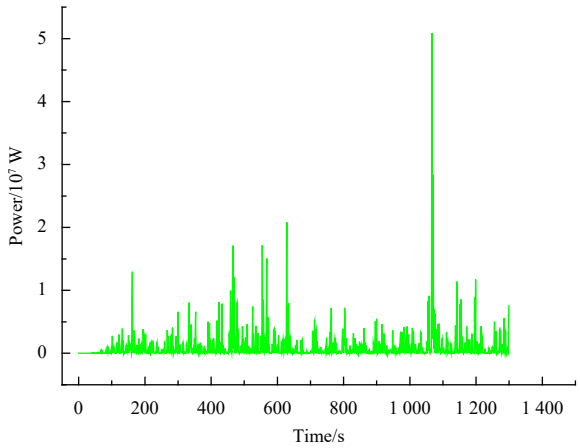

Fig. 12. WEC absorbed power time series under the sea state of nonlinear waves with H_S=12 m.

ectional JONSWAP wave spectrum with H_S=12 m, T_p=12 s, γ=1 and a cosine squared spreading function with the spreading parameter equal to 15. Figure 12 shows the predicted WEC absorbed power time series under the sea state of nonlinear irregular waves based on the same multi-directional JONSWAP wave spectrum with H_S=12 m, T_p=12 s, γ=1 and a cosine squared spreading function with the spreading parameter equal to 15. The calculation results in Figs 11 and 12 were obtained by solving the WEC nonlinear dynamic filter Eq. (17) in WEC-Sim. However, WEC-Sim does not have built-in functions for generating nonlinear irregular waves for calculating the wave excitation load $\boldsymbol{P}_{\text{ext}}(t)$ in Eq. (17). Therefore, this study externally generated nonlinear irregular waves by using the proposed second order random wave simulation method which imported into WEC-Sim. The nonlinear irregular wave simulation was started by taking the multi-directional JONSWAP wave spectrum (with H_S=12 m, T_p=12 s, γ=1) and integrating the energy over all directions to give the total energy at each frequency. The obtained equivalent frequency spectrum was then utilized to generate a nonlinear wave elevation time series of 1 200 points by applying Eqs (8) and (14). The generated nonlinear irregular waves time series were saved as a.mat file and then imported into WEC-Sim for calculating the wave excitation load $\boldsymbol{P}_{\text{ext}}(t)$ in Eq. (17) and subsequently obtaining the WEC absorbed power time series in Fig. 12. For comparison purpose, in this study, externally generated linear irregular waves by using Eqs (7) and (8) were also imported into WEC-Sim. The linear irregular wave simulation was started by

taking the multi-directional JONSWAP wave spectrum (with H_S=12 m, T_p=12 s, γ=1) and integrating the energy over all directions to give the total energy at each frequency. The obtained equivalent frequency spectrum was then utilized to generate a linear wave elevation time series of 1 200 points by applying Eqs (7) and (8). The generated linear irregular waves time series were saved as a .mat file and then imported into WEC-Sim for calculating the wave excitation load $\boldsymbol{P}_{\text{ext}}(t)$ in Eq. (17) and subsequently obtaining the WEC absorbed power time series in Fig. 11. Having obtained the prediction results as shown in Figs 11 and 12, the statistical characteristic values were subsequently calculated based on the time series shown in these two figures. Our calculation results are summarized in the last row in Table 1.

By carefully comparing and analyzing the calculation results, the mean value of the 1 200 s WEC absorbed power under the sea state of ideal linear irregular waves is smaller than the corresponding mean absorbed power value when inputting nonlinear irregular waves. In order to investigate the influences of choosing different significant wave height values on the power performances of wave energy converters, the aforementioned WEC absorbed power values were sequently calculated under 11 other sea states characterized with a multi-directional JONSWAP wave spectrum with the following parameters respectively: H_S=1 m, T_p=12 s, γ=1, s=15; H_S=2 m, T_p=12 s, γ=1, s=15; H_S=3 m, T_p=12 s, γ=1, s=15; H_S=4 m, T_p=12 s, γ=1, s=15; H_S=5 m, T_p=12 s, γ=1, s=15; H_S=6 m, T_p=12 s, γ=1, s=15; H_S=7 m, T_p=12 s, γ=1, s=15; H_S=8 m, T_p=12 s, γ=1, s=15; H_S=9 m, T_p=12 s, γ=1, s=15; H_S=10 m, T_p=12 s, γ=1, s=15; H_S=11 m, T_p=12 s, γ=1, s=15. The calculation results were also summarized in Table 1. By carefully comparing and analyzing these calculation results, in all these 11 sea states, the mean value of the 1 200 s WEC absorbed power under the sea state of ideal linear irregular waves is always smaller than the corresponding mean absorbed power value when inputting nonlinear irregular waves.

In order to further investigate the influences of using different random seed numbers for generating irregular waves on the power performances of wave energy converters, the aforementioned WEC absorbed power values were sequently calculated when inputting 11 different irregular wave elevation time series simulated based on the same multi-directional JONSWAP wave spectrum (H_S=12 m, T_p=12 s, γ=1, s=15) using different random seed numbers. The calculation results were summarized in Table 2. By carefully comparing and analyzing these calculation results, in all these 12 sea states, the mean value of the 1 200 s WEC absorbed power under the sea state of ideal linear irregular waves is always smaller than the corresponding mean absorbed power value when inputting nonlinear irregular waves. In one specific case (No. 11) the predicted WEC absorbed power value with the

Table 1. Predicted 1 200 s WEC absorbed power values at the sea states of T_p=16 s, γ=1, s=15

Statistical measures significant wave height/m	Mean value under sea state of linear waves/W	Mean value under sea state of second order nonlinear waves/W	Standard deviation value under sea state of linear waves/W	Standard deviation value under sea state of second order nonlinear waves/W	Sum value under sea state of linear waves/W	Sum value under sea state of second order nonlinear waves/W
1	138 437.041 16	138 511.458 57	147 967.477 21	148 037.483 74	$3.597\,98\times10^{8}$	$3.599\,91\times10^{8}$
2	183 201.455 43	183 729.925 15	219 208.088 86	219 533.048 23	$4.761\,41\times10^{8}$	$4.775\,14\times10^{8}$
3	199 926.337 33	199 983.502 74	249 739.808 07	251 762.625 93	$5.196\,09\times10^{8}$	$5.197\,57\times10^{8}$
4	274 600.575 60	276 111.716 03	403 700.408 94	408 900.025 58	$7.136\,87\times10^{8}$	$7.176\,14\times10^{8}$
5	315 077.752 10	316 133.239 68	454 553.945 21	454 063.308 63	$8.188\,87\times10^{8}$	$8.216\,30\times10^{8}$
6	433 808.094 51	444 136.336 28	726 265.219 59	769 908.283 18	$1.127\,47\times10^{9}$	$1.154\,31\times10^{9}$
7	490 131.331 53	503 258.637 00	776 567.662 95	809 812.456 90	$1.273\,85\times10^{9}$	$1.307\,97\times10^{9}$
8	594 029.946 90	621 211.754 87	978 890.289 27	$1.029\,46\times10^{6}$	$1.543\,88\times10^{9}$	$1.614\,53\times10^{9}$
9	796 963.826 65	874 346.209 99	$1.342\,61\times10^{6}$	$1.532\,51\times10^{6}$	$2.071\,31\times10^{9}$	$2.272\,43\times10^{9}$
10	767 280.020 13	825 077.575 89	$1.171\,64\times10^{6}$	$1.302\,27\times10^{6}$	$1.994\,16\times10^{9}$	$2.144\,38\times10^{9}$
11	$1.149\,2\times10^{6}$	$1.258\,1\times10^{6}$	$2.218\,24\times10^{6}$	$2.683\,45\times10^{6}$	$2.986\,80\times10^{9}$	$3.269\,80\times10^{9}$
12	$1.098\,6\times10^{6}$	$1.191\,8\times10^{6}$	$2.539\,72\times10^{6}$	$2.643\,26\times10^{6}$	$2.855\,25\times10^{9}$	$3.097\,48\times10^{9}$

Table 2. Predicted 1 200 s WEC absorbed power values at the sea states of H_S=12 m, T_p=16 s, γ=1, s=15

Statistical measures significant wave height/m	Mean value under sea state of linear waves/W	Mean value under sea state of second order nonlinear waves/W	Standard deviation value under sea state of linear waves/W	Standard deviation value under sea state of second order nonlinear waves/W	Sum value under sea state of linear waves/W	Sum value under sea state of second order nonlinear waves/W
12	$1.184\,85\times10^{6}$	$1.380\,75\times10^{6}$	$2.017\,13\times10^{6}$	$2.768\,39\times10^{6}$	$3.079\,41\times10^{9}$	$3.588\,57\times10^{9}$
12	$1.122\,70\times10^{6}$	$1.222\,33\times10^{6}$	$2.043\,28\times10^{6}$	$2.412\,29\times10^{6}$	$2.917\,91\times10^{9}$	$3.176\,85\times10^{9}$
12	$1.159\,23\times10^{6}$	$1.278\,71\times10^{6}$	$2.229\,10\times10^{6}$	$2.639\,01\times10^{6}$	$3.012\,85\times10^{9}$	$3.323\,36\times10^{9}$
12	$1.472\,23\times10^{6}$	$1.583\,50\times10^{6}$	$2.690\,01\times10^{6}$	$3.280\,96\times10^{6}$	$3.826\,32\times10^{9}$	$4.115\,50\times10^{9}$
12	$1.182\,07\times10^{6}$	$1.314\,31\times10^{6}$	$2.107\,16\times10^{6}$	$2.705\,89\times10^{6}$	$3.072\,19\times10^{9}$	$3.415\,88\times10^{9}$
12	$1.064\,10\times10^{6}$	$1.120\,36\times10^{6}$	$1.740\,52\times10^{6}$	$1.805\,26\times10^{6}$	$2.765\,60\times10^{9}$	$2.911\,83\times10^{9}$
12	$1.328\,98\times10^{6}$	$1.444\,81\times10^{6}$	$2.554\,03\times10^{6}$	$2.812\,90\times10^{6}$	$3.454\,03\times10^{9}$	$3.755\,06\times10^{9}$
12	$1.122\,96\times10^{6}$	$1.310\,56\times10^{6}$	$1.974\,89\times10^{6}$	$2.465\,68\times10^{6}$	$2.918\,57\times10^{9}$	$3.406\,15\times10^{9}$
12	$1.406\,60\times10^{6}$	$1.571\,63\times10^{6}$	$2.677\,32\times10^{6}$	$3.019\,67\times10^{6}$	$3.655\,75\times10^{9}$	$4.084\,66\times10^{9}$
12	$1.103\,65\times10^{6}$	$1.180\,66\times10^{6}$	$1.760\,90\times10^{6}$	$2.017\,55\times10^{6}$	$2.868\,38\times10^{9}$	$3.068\,53\times10^{9}$
12	$1.279\,46\times10^{6}$	$1.481\,30\times10^{6}$	$2.270\,87\times10^{6}$	$2.725\,54\times10^{6}$	$3.325\,31\times10^{9}$	$3.849\,90\times10^{9}$
12	$1.047\,26\times10^{6}$	$1.137\,99\times10^{6}$	$1.622\,24\times10^{6}$	$1.927\,67\times10^{6}$	$2.721\,84\times10^{9}$	$2.957\,64\times10^{9}$

nonlinear irregular waves as inputs is 15.8% larger than that predicted with the linear irregular waves as inputs. All the aforementioned calculation results highlight the vital importance of using the nonlinear irregular waves simulated based on a multi-directional wave spectrum when studying the power performances of wave energy converters.

5 Concluding remarks

In the present study the power performances of a two body point absorber WEC operating in a nonlinear multi-directional random sea have been rigorously investigated. The absorbed power of the WEC Power-Take-Off system has been predicted by incorporating a second order random wave model into a nonlinear dynamic filter. This is a new approach that is uniquely proposed to ocean wave energy research community. It has been demonstrated in this paper that the second order random wave model can be utilized to accurately simulate nonlinear irregular waves in a multi-directional sea. This will help us to avoid the inaccuracies resulting from using a first order linear wave model in the WEC simulation process. The predicted results in this paper have been systematically analyzed and compared, and the advantages of using our proposed new approach have been convincingly substantiated. The research findings in this paper highlight the vital importance of using the nonlinear irregular waves simulated based on a multi-directional wave spectrum when studying the power performances of wave energy converters. In the future if enough funding is secured, the proposed second order random wave simulation method will also be compared with the related WEC model physical test data in order to fully verify the accuracy of the model.

References

Fernandes M A, Fonseca N. 2013. Finite depth effects on the wave energy resource and the energy captured by a point absorber. Ocean Engineering, 67: 13–26, doi: 10.1016/j.oceaneng.2013.04.001

Lindgren G. 2015. Asymmetric waves in wave energy systems analysed by the stochastic Gauss–Lagrange wave model. Proceedings of the Estonian Academy of Sciences, 64(3): 291–296, doi: 10.3176/proc.2015.3.13

Manuel L, Nguyen P T T, Canning J, et al. 2018. Alternative approaches to develop environmental contours from Metocean data. Journal of Ocean Engineering and Marine Energy, 4(4): 293–310, doi: 10.1007/s40722-018-0123-0

Ochi M K. Ocean Waves: the Stochastic Approach. Cambridge: Cambridge University Press, 1998

Sirnivas S, Yu Y H, Hall M, et al. 2016. Coupled mooring analyses for the WEC-SIM wave energy converter design tool. In: Proceedings of the ASME 2016 35th International Conference on Ocean, Offshore and Arctic Engineering, Volume 6: Ocean Space Utilization. Busan, South Korea: ASME

Tom N M, Madhi F, Yeung R W. 2019. Power-to-load balancing for heaving asymmetric wave-energy converters with nonideal power take-off. Renewable Energy, 131: 1208–1225, doi: 10.1016/j.renene.2017.11.065

Tom N M, Yu Y H, Wright A D, et al. 2016. Balancing power absorption and fatigue loads in irregular waves for an oscillating surge wave energy converter. In: Proceedings of the ASME 2016 35th International Conference on Ocean, Offshore and Arctic Engineering, Volume 6: Ocean Space Utilization. Busan, South Korea: ASME

Tom N M, Yu Y H, Wright A D, et al. 2018. Balancing power absorption against structural loads with viscous drag and power-takeoff efficiency considerations. IEEE Journal of Oceanic Engineering, 43(4): 1048–1067, doi: 10.1109/JOE.2017.2764393

Wang Yingguang. 2014. Calculating crest statistics of shallow water nonlinear waves based on standard spectra and measured data at the Poseidon platform. Ocean Engineering, 87: 16–24, doi: 10.1016/j.oceaneng.2014.05.012

Wang Yingguang. 2018a. A novel simulation method for predicting power outputs of wave energy converters. Applied Ocean Research, 80: 37–48, doi: 10.1016/j.apor.2018.08.011

Wang Yingguang. 2018b. A novel method for predicting the power outputs of wave energy converters. Acta Mechanica Sinica, 34(4): 644–652, doi: 10.1007/s10409-018-0755-2

Wang Yingguang. 2019. Comparison of a Lagrangian and a Gaussian model for power output predictions in a random sea. Renewable Energy, 134: 426–435, doi: 10.1016/j.renene.2018.11.051

Wang Yingguang, Wang Lifu. 2018. Towards realistically predicting the power outputs of wave energy converters: Nonlinear simulation. Energy, 144: 120–128, doi: 10.1016/j.energy.2017.12.023